

## AGN-driven metallicity enrichment in the ISM of Mrk 573

D. L. KRÓL <sup>1,2</sup> P. ZHU <sup>1</sup> G. FABBIANO <sup>1</sup> M. ELVIS <sup>1</sup> L.J. KEWLEY <sup>1</sup> N. MURRAY <sup>3,4</sup> R. MIDDEI <sup>1</sup> AND  
A. TRINDADE FALCÃO <sup>5</sup>

<sup>1</sup>*Center for Astrophysics | Harvard & Smithsonian, 60 Garden Street, Cambridge, MA 02138, USA*

<sup>2</sup>*Astronomical Observatory of the Jagiellonian University, Orla 171, 30-244 Kraków, Poland*

<sup>3</sup>*Canadian Institute for Theoretical Astrophysics, University of Toronto, 60 Saint George Street, Toronto, ON M5S 3H8, Canada*

<sup>4</sup>*Canada Research Chair in Astrophysics, Canada*

<sup>5</sup>*NASA-Goddard Space Flight Center, Code 662, Greenbelt, MD 20771, USA*

### ABSTRACT

We present the first spatially resolved at  $\sim 20$  pc scale application of AGN-specific metallicity diagnostics for the nearby Compton-thick Seyfert 2 galaxy Mrk 573 ( $z = 0.017$ ). We use Hubble Space Telescope narrow-band imaging, MUSE integral-field spectroscopy and apply AGN strong-line metallicity diagnostics based on [O III], [S II], H $\beta$ , H $\alpha$ , and [N II] emission lines. We construct maps of  $12 + \log(\text{O}/\text{H})$  for two different metallicity calibrations and two different N/O–O/H scaling relations out to  $\sim 1$  kpc and down to  $\sim 20$  pc scales. Our analysis reveals metallicity enhancement in AGN-dominated regions, with oxygen abundances reaching up to few times Solar. The metallicity shows a patchy spatial distribution, varying on  $\sim 100$  pc scales, appears to trace the high Seyfert/LINER index (SLI) value regions and the VLA 6 cm jet/radio lobe emission. These spatial correspondences and the lack of evidence for star formation in the bicone region suggest that the enrichment originates from metals transported from the nuclear AGN regions by winds, outflows, or jets.

*Keywords:* Galaxies (573) — Interstellar medium (847) — Active galactic nuclei (16) — AGN host galaxies (2017) — Chemical abundances (224) — Metallicity (1031) — High Energy astrophysics (739)

### 1. INTRODUCTION

The metallicity of the interstellar medium (ISM) is usually associated with the chemical evolution of galaxies’ stellar populations (R. Maiolino & F. Mannucci 2019; L. J. Kewley et al. 2019). H II region metallicity diagnostics applied to large spectroscopic surveys revealed the stellar mass-metallicity relation, and showed that low-mass galaxies are more metal-poor and prone to metal loss, while massive systems retain or recycle their metals (C. A. Tremonti et al. 2004). Studies of individual galaxies have revealed negative radial O/H gradients with a universal slope (I. T. Ho et al. 2015).

The extent of Active Galactic Nuclei (AGN) influence on the chemical evolution of galaxies remains an open question. Several observations and simulations suggest that AGN activity can transport metals, either through jets (C. C. Kirkpatrick et al. 2009) or outflows (M. Villar Martín et al. 2024), out to  $\sim 10$  kpc. Cosmological

simulations indicate that jets and outflows can displace metal-rich gas from galaxies into the outskirts of clusters (D. Fabjan et al. 2010). M. Armah et al. (2024) showed an anti-correlation between the metallicity and Eddington ratio in the sample of nearby Seyfert galaxies. However, other observational studies probing radial metallicity profiles find no clear evidence of AGN impact (A. Amiri et al. 2025). Overall, the metallicity of AGN has been studied less extensively than that of star-forming galaxies. Only a few optical strong-line metallicity diagnostics were available for AGN, including theoretical calibrations (T. Storchi-Bergmann et al. 1998) and semi-empirical calibrations (C. S. Castro et al. 2017; S. P. Carvalho et al. 2020). The mass-metallicity relation in AGN host galaxies has been investigated, but it exhibits larger scatter than that observed in star-forming systems (A. D. Thomas et al. 2019; C. B. Oliveira et al. 2024), leaving open questions regarding the overall impact of AGN feedback on galactic chemical evolution.

In this paper, we leverage the new theoretical strong-line metallicity diagnostics suitable for photoioniza-

tion dominated (AGN-like) regions introduced by P. Zhu et al. (2024, Z24), and combine them with Hubble Space Telescope (*HST*) and MUSE data to study AGN-driven metal enrichment of the ISM. As no three-dimensional (3D) AGN photoionization models currently exist, the Z24 metallicity diagnostics are calibrated using one-dimensional (1D) AGN photoionization models of P. Zhu et al. (2023). While 1D models cannot capture the full anisotropic structure of the ISM, they have been shown to reproduce observed AGN emission-line spectra with reasonable accuracy and yield consistent predictions across UV, optical, and infrared wavelengths (P. Zhu et al. 2023). We present a detailed metallicity mapping of AGN-type regions in Mrk 573. Mrk 573 is a Compton-thick AGN (absorbed by the equivalent column density  $> 1.6 \times 10^{24} \text{ cm}^{-2}$  M. Guainazzi et al. 2005) hosted by a Seyfert 2 galaxy at  $z = 0.017$  (scale  $\sim 0.35 \text{ kpc}''$ , C. M. Springob et al. 2005). The extended emission in Mrk 573 has been studied across wavelengths, from deep X-ray *Chandra* observations of hot plasma emission (A. Paggi et al. 2012; S. Bianchi et al. 2010), through *HST* and *Gemini* optical and infrared observations of ionized gas (T. C. Fischer et al. 2010, 2017), down to *VLA* radio observations of the jet and radio lobes at 6 cm (J. S. Ulvestad & A. S. Wilson 1984).

Using optical emission line diagnostics, we categorize Mrk 573 Narrow Line Regions (NLR) as Seyfert(AGN)- or LINER-type dominated. Then, based on two different metallicity diagnostics (Z24) we map the ISM metallicity up to  $\sim 1.0 \text{ kpc}$  from the nucleus, resolving  $\sim 20 \text{ pc}$  scales for AGN-type emission. We show that the metallicity is enriched in the ionization bicone regions, and  $\log(\text{O}/\text{H})$  values trace 6 cm radio contours, and the ISM excitation using the recently developed Seyfert/LINER index (SLI, D. L. Król et al. 2025). In Sec. 2 we introduce the data sets and analysis methods, and present the VO (Veilleux & Osterbrock, S. Veilleux & D. E. Osterbrock 1987) diagnostic diagrams and map for Mrk 573. In Sec. 3 we present the metallicity maps. In Sec. 4 we discuss potential sources of metal enrichment. In Sec. 5 we summarize our conclusions.

Through the paper, we use  $\Lambda$ CDM cosmology with  $H_0 = 69.3 \text{ kms}^{-1}\text{Mpc}^{-1}$  and  $\Omega_m = 0.287$  (G. Hinshaw et al. 2013).

## 2. DATA AND ANALYSIS

### 2.1. Data

We used archival *HST* observations in key diagnostic lines,  $[\text{O III}]\lambda 5007$ ,  $\text{H}\alpha + [\text{N II}]\lambda\lambda 6548, 83$ ,  $\text{H}\beta$ , and

$[\text{S II}]\lambda\lambda 6717, 31^6$ , in the narrow-band filters FR533N, FR680N, FR656N, and FR505N, respectively, characterized by  $0.05''$  resolution (see J. Ma et al. 2021 for details).

To disentangle the fluxes of the  $\text{H}\alpha$  and  $[\text{N II}]$  emission lines we used the Very Large Telescope/MUSE integral field unit (IFU) data. Mrk 573 was observed with MUSE on January 24th 2021, with 72 min total exposure time on the wavelengths covering the range of  $4650\text{-}9300\text{\AA}$  (R. Bacon et al. 2010). Observations were carried out for the  $1.53' \times 1.53'$  field of view, with  $0.2''$  spatial resolution and seeings' full width half maximum of  $1.593''$ . For the data analysis we followed P. Zhu et al. (2025) approach, and performed single Gaussian fits to the emission lines using the penalized pixel-fitting routine module (M. Cappellari & E. Emsellem 2004; M. Cappellari 2017) incorporated in the nGIST pipeline (A. Bittner et al. 2019)<sup>7</sup>.

### 2.2. VO mapping

The distinction between star-forming, AGN-dominated, and low-ionization nuclear emission-line region (LINER) dominated galaxies is based on the BPT (Baldwin, Phillips & Terlevich, J. A. Baldwin et al. 1981; L. J. Kewley et al. 2006) and VO diagrams (S. Veilleux & D. E. Osterbrock 1987). Using spatially resolved data, BPT/VO maps can be built to determine the dominating driver of line emission in different regions within the same galaxy (W. P. Maksym et al. 2016; J. Ma et al. 2021). We used here VO diagrams/maps which are based on a comparison of the  $[\text{O III}]/\text{H}\beta$  and  $[\text{S II}]/\text{H}\alpha$  flux ratios. With the *HST* data, such analyses can be performed at  $\sim 0.1''$  scales (W. P. Maksym et al. 2016), corresponding to the linear scales of tens of parsecs in the nearest AGN (J. Ma et al. 2021; W. P. Maksym et al. 2021; A. Trindade Falcão et al. 2025).

In the BPT and VO diagrams AGN-type (Seyfert-type) emission is typically attributed to AGN photoionization excitation, though it can also be produced by fast shocks with a photo-ionizing precursor (M. G. Allen et al. 2008). The LINER-type emission can be associated with a variety of mechanisms, including post-asymptotic giant branch stars (L. Binette et al. 1994; G. Stasińska et al. 2008), low-luminosity/obscured AGN radiation (J. P. Halpern & J. E. Steiner 1983; S. B. Kraemer et al. 2008) and shock excitation (J. P. Halpern & J. E. Steiner 1983; M. A. Dopita & R. S. Sutherland

<sup>6</sup> Data set DOI:10.17909/ksh5-7168

<sup>7</sup> <http://ascl.net/1907.025>

1995). The last two are the most likely in the central regions of Seyfert galaxy (J. Ma et al. 2021).

### 2.3. SLI mapping

The VO mapping can be extended to spatially probe the local small-scale variations of the ISM excitation, rather than to rely on a simple LINER/Seyfert dichotomy. SLI is calculated on a pixel-by-pixel basis as the Seyfert and LINER type pixel perpendicular distance to the Seyfert/LINER division line (D. Ł. Król et al. 2025).

We constructed the VO diagram for Mrk 573 and separated AGN- and LINER-type emission by comparing the values of  $\log([\text{O III}]/\text{H}\beta)$  and  $\log([\text{S II}]/\text{H}\alpha)$  (L. J. Kewley et al. 2006). Fluxes were calculated pixel-by-pixel, only for pixels with narrow-band filter fluxes at or above the  $3\sigma$  level, where  $\sigma$  is the standard deviation of the pixel count in a background-dominated region (J. Ma et al. 2021). We color-coded both the map and VO diagram based on the SLI value. The uncertainties are derived using the standard error propagation formula for uncorrelated variables (see Appendix B in D. Ł. Król et al. 2025, for details), assuming that  $\sigma$  represents the uncertainty for each individual filter observation. The SLI map and the corresponding diagram in Fig. 1 show more structure than a simple Seyfert/LINER map. We color-code SLI values on both the VO map and the diagram. By construction, LINER points (in blue) have  $\text{SLI} < 0$ , and Seyfert points (in red) have  $\text{SLI} > 0$ . The black contour in the left panel represents points that lie on the Seyfert/LINER division line ( $\text{SLI} = 0$ ). In agreement with the results of J. Ma et al. (2021), the nucleus and ionization bicone are dominated by Seyfert-like activity. Surrounding it, a thin LINER “cocoon” ( $\sim 100$  pc) is characterized by intermediate SLI values, transitioning further into LINER-type emission with  $\text{SLI} < -0.2$ .

### 2.4. Metallicity diagnostics

To calculate  $\log(\text{O}/\text{H})$  we used the metallicity diagnostics presented in Z24 for AGN-type emission with MAPPINGS V (R. Sutherland et al. 2018), which use incident AGN spectral energy distribution generated based on *OXAF* (A. D. Thomas et al. 2016), a simplified version of *OPTXAGNF* (C. Done et al. 2012; C. Jin et al. 2012) for thin-disk accretion.

We applied two metallicity diagnostics, both strongly dependent on the gas-phase metallicity,  $\log(\text{O}/\text{H})$ , but not on other gas parameters such as the ionization parameter,  $\log U$ , gas pressure, and the peak energy of the AGN SED,  $E_p$ . They are given by the following line

ratios:

$$\begin{aligned} R1 &= \log R(N2, S2, \text{H}\alpha) = \\ &= \log \left( \frac{[\text{N II}]\lambda 6584}{[\text{S II}]\lambda\lambda 6717, 31} \right) \\ &+ 0.264 \log \left( \frac{[\text{N II}]\lambda 6584}{\text{H}\alpha} \right) \end{aligned} \quad (1)$$

and

$$\begin{aligned} R2 &= \log R(N2, S2, \text{O}3) = \\ &= 0.9738 \log \left( \frac{[\text{N II}]\lambda 6584}{[\text{S II}]\lambda\lambda 6717, 31} \right) \\ &+ 0.047 \log \left( \frac{[\text{N II}]\lambda 6584}{\text{H}\alpha} \right) \\ &- 0.183 \log \left( \frac{[\text{O III}]\lambda 5007}{\text{H}\beta} \right). \end{aligned} \quad (2)$$

Both diagnostics are based on ratios of lines very close in the wavelength, ensuring limited impact of the dust extinction on the results.

We constructed metallicity maps for two N/O-O/H scaling relations (B. A. Groves et al. 2004; O. L. Dors et al. 2017) corresponding to the galaxies’ different star formation history: “low”,  $\log(\text{N}/\text{O}) = \log(10^{-1.732} + 10^{\log(\text{O}/\text{H})+2.19})$ , and “high”,  $\log(\text{N}/\text{O}) = 1.29 \times (12 + \log(\text{O}/\text{H}) - 11.84)$ . We derived the  $\log(\text{O}/\text{H})$  uncertainties using the standard error propagation formula, combining the individual filter measurement errors,  $\sigma$ , with the diagnostics’ RMS (see Table 4 in Z24).

Depending on the origin of the LINER-type emission, its metallicity can be approximated either using diagnostic methods similar to those for AGN-type emission, or using diagnostics derived for shock-excited regions, in the cases of obscured AGN radiation and shock-driven emission, respectively (J. P. Halpern & J. E. Steiner 1983; M. A. Dopita & R. S. Sutherland 1995). We use both approaches. We approximate LINER-type regions average metallicity by applying the AGN-type diagnostics (Eq. 1,2) for the photoionization excitation and in the shock-driven emission scenario (Zhu et al., in preparation).

### 2.5. Metallicity maps

Based on the SLI map we separated AGN- and LINER-type-dominated regions. For Seyfert-dominated regions, we calculated R1 and R2 values on a pixel-by-pixel basis and then inserted them into the theoretically derived metallicity diagnostics to calculate  $\log(\text{O}/\text{H})$  (Tab. 4 in Z24). We adopted  $\log(E_p/\text{keV}) = -1.5$  and the  $\log U$  values by Zhu et al. (in preparation), derived based on *MUSE*-observed  $[\text{O III}]/[\text{O I}]$  emission line ratios and Z24 line diagnostics. We confirmed that derived metallicities are insensitive to  $E_p$  and  $\log U$  by

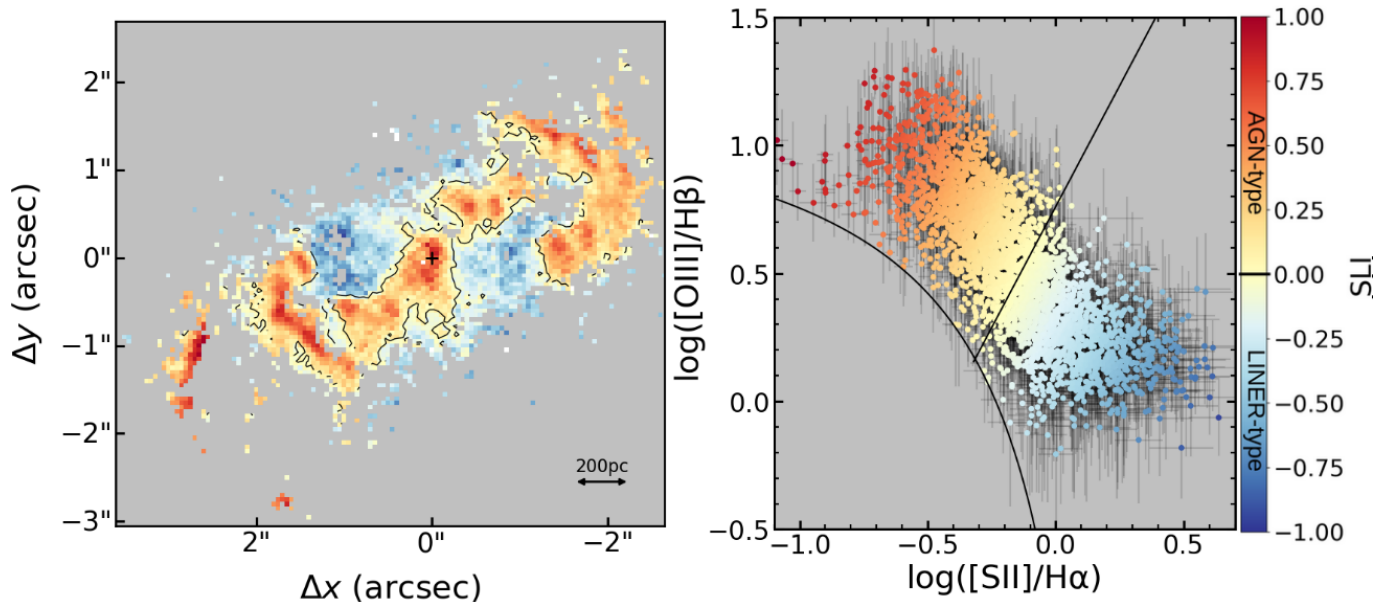


**Figure 1.** SLI map and diagram for Mrk 573. Left panel: SLI map, with colors reflecting SLI values, i.e. the distance of each pixel from the Seyfert/LINER division line in the VO diagram. Black contours trace points on the Seyfert/LINER division line (SLI=0). The black “X” marks the position of the nucleus. Right panel: corresponding VO diagram, with red indicating Seyfert-like excitation and blue denoting LINER-like excitation. The color intensity scales with the SLI value.

testing a range of values. This is consistent with Z24. The mean value of  $12 + \log(\text{O}/\text{H})$  uncertainties derived using the standard error propagation formula for uncorrelated variables is  $\sim 0.035$  dex.

### 3. RESULTS

Fig. 2 shows the metallicity maps, represented as  $12 + \log(\text{O}/\text{H})$ , for the *R1* (upper panels of Fig. 2) and *R2* (lower panels of Fig. 2) diagnostics. Both the “low” (left panels of Fig. 2) and “high” (right panels of Fig. 2)  $\text{N}/\text{O}-\text{O}/\text{H}$  scalings consistently show metal enrichment in AGN-type regions. Surprisingly, we find enhanced, super-solar metallicity associated with the extended AGN excitation regions of Mrk 573. For both scaling relations some areas reach values up to  $5\times$  Solar for the “low”  $\text{N}/\text{O}-\text{O}/\text{H}$  scaling (assuming  $12 + \log(\text{O}/\text{H}) = 8.75$  for the Solar value, M. Bergemann et al. 2021). The  $\log(\text{O}/\text{H})$  distribution within the bi-cone areas shows features on  $\sim 100$  pc scales. High metallicity appears to trace the high SLI values, radio emission at 6 cm and the X-ray emission (shown as black contours in Fig. 2). We note that other theoretical diagnostics are known to overestimate metallicities by  $\sim 0.2$  dex compared to direct methods (O. L. Dors et al. 2020). The presence of regions with super-solar metallicity would not be affected by a similar offset in the Z24 diagnostic.

The metallicity of AGN-type regions is enhanced with respect to the LINER-type regions (blue in Fig. 1). The mean  $\log(\text{O}/\text{H})$  of LINER regions is  $\sim 0.35$  dex lower

for both the photoionized (R1/R2) and shock based diagnostics (Zhu et al. 2026, in preparation, Z26). The LINER-type points roughly follow the  $12 + \log(\text{O}/\text{H})$  and SLI correlation seen for the AGN-type points.

As reported by R. A. Riffel et al. (2021), emission within the inner kpc may be partially shock-induced, potentially biasing gas properties derived from photoionization diagnostics. However, our tests show that the results are robust to shock contributions in the bi-cone regions, with shock-based diagnostics (Z26) resulting in similar results.

### 4. DISCUSSION

What is the origin of the enhanced metallicity associated with the AGN excited ISM (Fig. 2)?

The metal enrichment can be either (1) created within the ionization bi-cones or (2) entrained by winds, outflows, or jets. Since there is no evidence of star formation within the ionization bi-cones (J. Ma et al. 2021), the observed enrichment is unlikely to originate from in-situ stellar processes.

The central AGN regions, instead, are an appealing source of metals, as their broad-line regions (BLRs) are known to exhibit super-solar abundances (F. Hamann & G. Ferland 1999). According to recent results, accretion disks are expected to be populated by stars, either formed in the accretion disk or captured (G. Fabj et al. 2025). Metals created in the disk/torus would then have to be transported to scales of up to a few kiloparsecs.

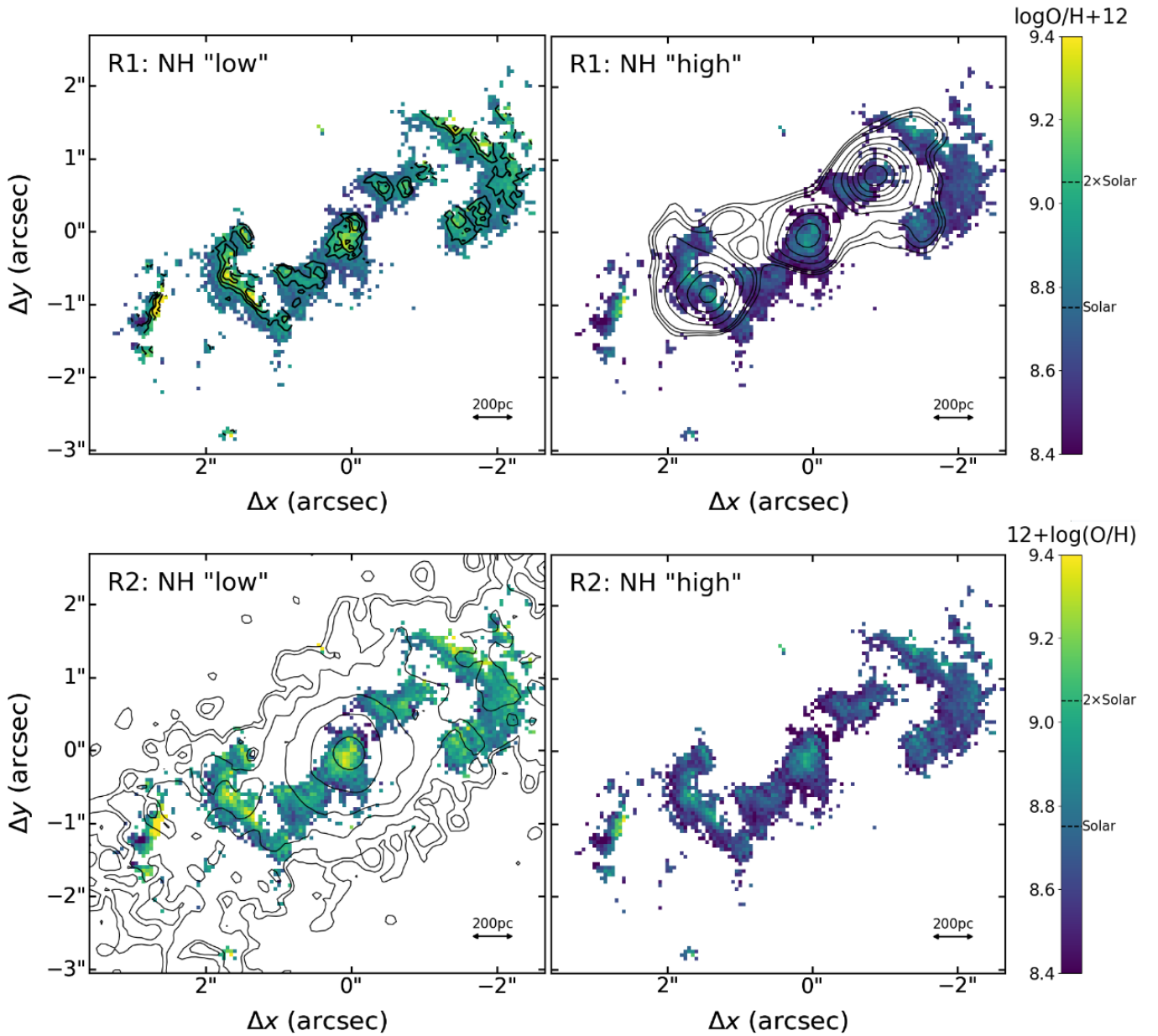


**Figure 2.** Metallicity ( $\log(\text{O}/\text{H}) + 12$ ) maps calculated for AGN-type regions, based on R1 (upper row) and R2 (lower row) metallicity diagnostics and assuming low (left panels) and high (right panels) nitrogen scaling relations. Black contours trace SLI value on the top-left panel, 6 cm radio jet/radio-lobes emission and soft (0.3-2.0 keV) Chandra X-ray emission in bottom-left panel. Dashed lines on the color scale mark Solar, 2×Solar and 5×Solar abundances (assuming  $12 + \log(\text{O}/\text{H}) = 8.75$  for the Solar value, [M. Bergemann et al. 2021](#)).

Below we briefly discuss two possible metal transportation mechanisms.

#### 4.1. Enrichment via winds and outflows

The first possibility is that metals are carried outward by AGN-driven winds and outflows into the bi-cone regions. Recent *JWST* observations of massive outflows in radio-loud AGN ([R. A. Riffel et al. 2025](#)) provide evidence of the impact of AGN outflows on the bi-cone ISM. Other studies support AGN-driven outflows prevalence

(e.g., [A. Deconto-Machado et al. 2022](#); [M. Revalski et al. 2025](#)).

In particular, outflows with velocities up to  $\sim 1000 \text{ km s}^{-1}$  and  $\dot{M}_{obs} \sim 1 M_{\odot} \text{ yr}^{-1}$  mass outflow rates have been found up to  $\sim 1 \text{ kpc}$  from the Mrk 573 nucleus ([M. Revalski et al. 2018](#)). Following the approach of [M. Cano-Díaz et al. \(2012\)](#), we estimated the mass of the emitting gas in AGN-type regions as:

$$M = 5.3 \times 10^7 \frac{L_{44}([\text{O III}])}{n_{e3}Z} M_{\odot} = (3-5) \times 10^5 M_{\odot}, \quad (3)$$

with  $Z$  denoting the oxygen abundance in Solar units,  $n_{e3}$  the electron density of the gas in units of  $10^3 \text{ cm}^{-3}$ , and  $L_{44}([\text{O III}])$  the  $[\text{O III}]$  luminosity in units of  $10^{44} \text{ erg s}^{-1}$ . Based on  $[\text{S II}]_{\lambda\lambda 6716, 673 \text{ \AA}}$  fluxes measured by *MUSE*, we estimated  $n_{e3}$  following R. L. Sanders et al. (2016) method. The mass of the gas is calculated on a pixel-by-pixel basis using the  $[\text{O III}]$  emission, metallicity and  $n_{e3}$  maps. Derived mass together with measured  $\dot{M}_{obs}$  indicate timescales of  $\sim 3 \times 10^5$  yrs needed to displace metals from the AGN central regions to the NLR. These timescales match the time needed to reach  $\sim 1$  kpc radius at  $1000 \text{ km s}^{-1}$  velocity.

Can radiation driven winds move that much matter? The bolometric luminosity,  $L_{bol}$ , of Mrk 573 is  $5.2 \times 10^{41} \text{ erg s}^{-1}$  (O. Gonzalez-Martin et al. 2010). For the outflow velocity,  $v_w = 1000 \text{ km s}^{-1}$  the mass rate of a radiation driven wind is:

$$\dot{M}_w = \frac{L_{bol}}{c v_w} \sim 2.8 M_{\odot} \text{ yr}^{-1}. \quad (4)$$

Assuming a covering factor of  $\sim 0.5$  the derived  $\dot{M}_w$  is consistent with  $\dot{M}_{obs}$ .

#### 4.2. Enrichment via Jets

In the second scenario, jets play an important role in detection of metal enrichment. This may be the case in Mrk 573, since there is radio emission in the metal-enriched areas (Fig. 2, right panels).

Jet-associated metal displacement has been seen before, e.g., in the Hydra A galaxy (C. C. Kirkpatrick et al. 2009). Theoretical and numerical considerations, although in the context of galaxy clusters, show that jets may drag up to  $\sim 10^8$ – $10^9 M_{\odot}$  of gas (D. S. De Young 1986; A. Simionescu et al. 2009; E. C. D. Pope et al. 2010), well above our estimated mass of the metal-enriched gas.

The jet kinetic power,  $P_j$  can be estimated as  $\sim 4 \times 10^{41} \text{ erg s}^{-1}$  based on its luminosity at 1.4 GHz,  $L_{1.4}$  (see K. W. Cavagnolo et al. 2010). We adopted  $L_{1.4} = 2.48 \times 10^{-2} \text{ Jy}$  (J. J. Condon et al. 1998). The kinetic luminosity of the  $M \sim 5 \times 10^5 M_{\odot}$  gas moving with  $v_m = 1000 \text{ km s}^{-1}$  velocity can be estimated as  $\sim 2 \times 10^{41} \text{ erg s}^{-1}$ , therefore based on the energetics alone, jet could move that amount of gas.

More importantly, jet-induced shocks in Mrk 573 may play an important role in the metal-enrichment if it originates from dust outflows, such as those found in high-redshift galaxies (A. Vayner et al. 2025). Metal-rich dust can be pushed from the AGN torus into the bi-cone areas, where shocks and photoionization may destroy it and release the metals in the ISM, see the “engulfed cloud” model, invoked as one of the scenarios explaining the absorption features in Compact Symmetric Objects (CSOs, M. C. Begelman 1999). This scenario could explain the correlation between  $\log(\text{O}/\text{H})$  and SLI, as high SLI values seem to correlate with the presence of fast shocks (D. L. Król et al. 2025).

## 5. SUMMARY AND CONCLUSION

In this paper we report metal enrichment in the AGN-type bi-cone areas of Mrk 573. Enrichment is seen in  $\log(\text{O}/\text{H})$  derived with both theoretical metallicity diagnostics and with N/O–O/H scaling relations, with  $\log(\text{O}/\text{H})$  values reaching up to five times the Solar value for the “low” N/O–O/H scaling relation. Considering both the AGN photo-ionized and shock origin for LINER-type regions, the derived metallicity values are higher in AGN-type regions than in LINER-type regions.

The  $\log(\text{O}/\text{H})$  values trace the SLI values, soft X-ray emission and 6 cm radio emission, which indicates a strong link between the metal enrichment and the AGN-type emission mechanism, and we discussed potential avenues of metal-enriched gas transportation from the active nucleus to the NLR region: (1) metal-rich outflows, jet/radio-lobe-driven (2) metal displacement, and the possible role of associated shocks in releasing metals bound in dust outflows from the torus.

The distinction between these mechanisms can be made through detailed studies of other objects. A similar metallicity enrichment is seen in other seven nearby Seyfert 2 galaxies. Future analysis will include application of theoretical diagnostics to *HST* and *MUSE* data, and comparison of a larger sample of Seyfert 2 galaxies with X-ray, radio and IR emission (Król, et al. 2026 in preparation, Zhu et al. 2026 in preparation).

## ACKNOWLEDGMENTS

*Facilities:* HST, CXO, VLA, MUSE

*Software:* Astropy (Astropy Collaboration et al. 2022, 2018, 2013)

## REFERENCES

- Allen, M. G., Groves, B. A., Dopita, M. A., Sutherland, R. S., & Kewley, L. J. 2008, *ApJS*, 178, 20, doi: [10.1086/589652](https://doi.org/10.1086/589652)
- Amiri, A., Knapen, J. H., Lehmer, B. D., & Khoram, A. 2025, arXiv e-prints, arXiv:2509.12156, doi: [10.48550/arXiv.2509.12156](https://doi.org/10.48550/arXiv.2509.12156)
- Armah, M., Riffel, R., Dahmer-Hahn, L. G., et al. 2024, *MNRAS*, 534, 2723, doi: [10.1093/mnras/stae2263](https://doi.org/10.1093/mnras/stae2263)
- Astropy Collaboration, Robitaille, T. P., Tollerud, E. J., et al. 2013, *A&A*, 558, A33, doi: [10.1051/0004-6361/201322068](https://doi.org/10.1051/0004-6361/201322068)
- Astropy Collaboration, Price-Whelan, A. M., Sipőcz, B. M., et al. 2018, *AJ*, 156, 123, doi: [10.3847/1538-3881/aabc4f](https://doi.org/10.3847/1538-3881/aabc4f)
- Astropy Collaboration, Price-Whelan, A. M., Lim, P. L., et al. 2022, *ApJ*, 935, 167, doi: [10.3847/1538-4357/ac7c74](https://doi.org/10.3847/1538-4357/ac7c74)
- Bacon, R., Accardo, M., Adjali, L., et al. 2010, in *Society of Photo-Optical Instrumentation Engineers (SPIE) Conference Series*, Vol. 7735, *Ground-based and Airborne Instrumentation for Astronomy III*, ed. I. S. McLean, S. K. Ramsay, & H. Takami, 773508, doi: [10.1117/12.856027](https://doi.org/10.1117/12.856027)
- Baldwin, J. A., Phillips, M. M., & Terlevich, R. 1981, *PASP*, 93, 5, doi: [10.1086/130766](https://doi.org/10.1086/130766)
- Begelman, M. C. 1999, in *The Most Distant Radio Galaxies*, ed. H. J. A. Röttgering, P. N. Best, & M. D. Lehnert, 173
- Bergemann, M., Hoppe, R., Semenova, E., et al. 2021, *MNRAS*, 508, 2236, doi: [10.1093/mnras/stab2160](https://doi.org/10.1093/mnras/stab2160)
- Bianchi, S., Chiaberge, M., Evans, D. A., et al. 2010, *MNRAS*, 405, 553, doi: [10.1111/j.1365-2966.2010.16475.x](https://doi.org/10.1111/j.1365-2966.2010.16475.x)
- Binette, L., Magris, C. G., Stasińska, G., & Bruzual, A. G. 1994, *A&A*, 292, 13
- Bittner, A., Falcón-Barroso, J., Nedelchev, B., et al. 2019, *A&A*, 628, A117, doi: [10.1051/0004-6361/201935829](https://doi.org/10.1051/0004-6361/201935829)
- Cano-Díaz, M., Maiolino, R., Marconi, A., et al. 2012, *A&A*, 537, L8, doi: [10.1051/0004-6361/201118358](https://doi.org/10.1051/0004-6361/201118358)
- Cappellari, M. 2017, *MNRAS*, 466, 798, doi: [10.1093/mnras/stw3020](https://doi.org/10.1093/mnras/stw3020)
- Cappellari, M., & Emsellem, E. 2004, *PASP*, 116, 138, doi: [10.1086/381875](https://doi.org/10.1086/381875)
- Carvalho, S. P., Dors, O. L., Cardaci, M. V., et al. 2020, *MNRAS*, 492, 5675, doi: [10.1093/mnras/staa193](https://doi.org/10.1093/mnras/staa193)
- Castro, C. S., Dors, O. L., Cardaci, M. V., & Hägele, G. F. 2017, *MNRAS*, 467, 1507, doi: [10.1093/mnras/stx150](https://doi.org/10.1093/mnras/stx150)
- Cavagnolo, K. W., McNamara, B. R., Nulsen, P. E. J., et al. 2010, *ApJ*, 720, 1066, doi: [10.1088/0004-637X/720/2/1066](https://doi.org/10.1088/0004-637X/720/2/1066)
- Condon, J. J., Cotton, W. D., Greisen, E. W., et al. 1998, *AJ*, 115, 1693, doi: [10.1086/300337](https://doi.org/10.1086/300337)
- De Young, D. S. 1986, *ApJ*, 307, 62, doi: [10.1086/164393](https://doi.org/10.1086/164393)
- Deconto-Machado, A., Riffel, R. A., Ilha, G. S., et al. 2022, *A&A*, 659, A131, doi: [10.1051/0004-6361/202140613](https://doi.org/10.1051/0004-6361/202140613)
- Done, C., Davis, S. W., Jin, C., Blaes, O., & Ward, M. 2012, *MNRAS*, 420, 1848, doi: [10.1111/j.1365-2966.2011.19779.x](https://doi.org/10.1111/j.1365-2966.2011.19779.x)
- Dopita, M. A., & Sutherland, R. S. 1995, *ApJ*, 455, 468, doi: [10.1086/176596](https://doi.org/10.1086/176596)
- Dors, O. L., Maiolino, R., Cardaci, M. V., et al. 2020, *MNRAS*, 496, 3209, doi: [10.1093/mnras/staa1781](https://doi.org/10.1093/mnras/staa1781)
- Dors, Jr., O. L., Arellano-Córdova, K. Z., Cardaci, M. V., & Hägele, G. F. 2017, *MNRAS*, 468, L113, doi: [10.1093/mnrasl/slx036](https://doi.org/10.1093/mnrasl/slx036)
- Fabj, G., Dittmann, A. J., Cantiello, M., Perna, R., & Samsing, J. 2025, *ApJ*, 981, 16, doi: [10.3847/1538-4357/ada896](https://doi.org/10.3847/1538-4357/ada896)
- Fabjan, D., Borgani, S., Tornatore, L., et al. 2010, *MNRAS*, 401, 1670, doi: [10.1111/j.1365-2966.2009.15794.x](https://doi.org/10.1111/j.1365-2966.2009.15794.x)
- Fischer, T. C., Crenshaw, D. M., Kraemer, S. B., Schmitt, H. R., & Trippe, M. L. 2010, *AJ*, 140, 577, doi: [10.1088/0004-6256/140/2/577](https://doi.org/10.1088/0004-6256/140/2/577)
- Fischer, T. C., Machuca, C., Diniz, M. R., et al. 2017, *ApJ*, 834, 30, doi: [10.3847/1538-4357/834/1/30](https://doi.org/10.3847/1538-4357/834/1/30)
- Gonzalez-Martin, O., Acosta-Pulido, J. A., Perez Garcia, A. M., & Ramos Almeida, C. 2010, *ApJ*, 723, 1748, doi: [10.1088/0004-637X/723/2/1748](https://doi.org/10.1088/0004-637X/723/2/1748)
- Groves, B. A., Dopita, M. A., & Sutherland, R. S. 2004, *ApJS*, 153, 75, doi: [10.1086/421114](https://doi.org/10.1086/421114)
- Guainazzi, M., Matt, G., & Perola, G. C. 2005, *A&A*, 444, 119, doi: [10.1051/0004-6361:20053643](https://doi.org/10.1051/0004-6361:20053643)
- Halpern, J. P., & Steiner, J. E. 1983, *ApJL*, 269, L37, doi: [10.1086/184051](https://doi.org/10.1086/184051)
- Hamann, F., & Ferland, G. 1999, *ARA&A*, 37, 487, doi: [10.1146/annurev.astro.37.1.487](https://doi.org/10.1146/annurev.astro.37.1.487)
- Hinshaw, G., Larson, D., Komatsu, E., et al. 2013, *ApJS*, 208, 19, doi: [10.1088/0067-0049/208/2/19](https://doi.org/10.1088/0067-0049/208/2/19)
- Ho, I. T., Kudritzki, R.-P., Kewley, L. J., et al. 2015, *MNRAS*, 448, 2030, doi: [10.1093/mnras/stv067](https://doi.org/10.1093/mnras/stv067)
- Jin, C., Ward, M., Done, C., & Gelbord, J. 2012, *MNRAS*, 420, 1825, doi: [10.1111/j.1365-2966.2011.19805.x](https://doi.org/10.1111/j.1365-2966.2011.19805.x)
- Kewley, L. J., Groves, B., Kauffmann, G., & Heckman, T. 2006, *MNRAS*, 372, 961, doi: [10.1111/j.1365-2966.2006.10859.x](https://doi.org/10.1111/j.1365-2966.2006.10859.x)
- Kewley, L. J., Nicholls, D. C., & Sutherland, R. S. 2019, *ARA&A*, 57, 511, doi: [10.1146/annurev-astro-081817-051832](https://doi.org/10.1146/annurev-astro-081817-051832)
- Kirkpatrick, C. C., Gitti, M., Cavagnolo, K. W., et al. 2009, *ApJL*, 707, L69, doi: [10.1088/0004-637X/707/1/L69](https://doi.org/10.1088/0004-637X/707/1/L69)
- Kraemer, S. B., Schmitt, H. R., & Crenshaw, D. M. 2008, *ApJ*, 679, 1128, doi: [10.1086/587802](https://doi.org/10.1086/587802)

- Król, D. L., Fabbiano, G., Elvis, M., et al. 2025, arXiv e-prints, arXiv:2510.22447, doi: [10.48550/arXiv.2510.22447](https://doi.org/10.48550/arXiv.2510.22447)
- Ma, J., Maksym, W. P., Fabbiano, G., et al. 2021, *ApJ*, 908, 155, doi: [10.3847/1538-4357/abcfc1](https://doi.org/10.3847/1538-4357/abcfc1)
- Maiolino, R., & Mannucci, F. 2019, *A&A Rv*, 27, 3, doi: [10.1007/s00159-018-0112-2](https://doi.org/10.1007/s00159-018-0112-2)
- Maksym, W. P., Fabbiano, G., Elvis, M., et al. 2016, *ApJ*, 829, 46, doi: [10.3847/0004-637X/829/1/46](https://doi.org/10.3847/0004-637X/829/1/46)
- Maksym, W. P., Fabbiano, G., Elvis, M., et al. 2021, *ApJ*, 917, 85, doi: [10.3847/1538-4357/ac0976](https://doi.org/10.3847/1538-4357/ac0976)
- Oliveira, C. B., Dors, O., Zinchenko, I., et al. 2024, *PASA*, 41, e099, doi: [10.1017/pasa.2024.110](https://doi.org/10.1017/pasa.2024.110)
- Paggi, A., Wang, J., Fabbiano, G., Elvis, M., & Karovska, M. 2012, *ApJ*, 756, 39, doi: [10.1088/0004-637X/756/1/39](https://doi.org/10.1088/0004-637X/756/1/39)
- Pope, E. C. D., Babul, A., Pavlovski, G., Bower, R. G., & Dotter, A. 2010, *MNRAS*, 406, 2023, doi: [10.1111/j.1365-2966.2010.16816.x](https://doi.org/10.1111/j.1365-2966.2010.16816.x)
- Revalski, M., Crenshaw, D. M., Kraemer, S. B., et al. 2018, *ApJ*, 856, 46, doi: [10.3847/1538-4357/aab107](https://doi.org/10.3847/1538-4357/aab107)
- Revalski, M., Crenshaw, D. M., Polack, G. E., et al. 2025, *ApJ*, 984, 32, doi: [10.3847/1538-4357/adc131](https://doi.org/10.3847/1538-4357/adc131)
- Riffel, R. A., Dors, O. L., Armah, M., et al. 2021, *MNRAS*, 501, L54, doi: [10.1093/mnras/slaa194](https://doi.org/10.1093/mnras/slaa194)
- Riffel, R. A., Melo-Carneiro, C. R., Souza-Oliveira, G. L., et al. 2025, *A&A*, 701, L11, doi: [10.1051/0004-6361/202556329](https://doi.org/10.1051/0004-6361/202556329)
- Sanders, R. L., Shapley, A. E., Kriek, M., et al. 2016, *ApJ*, 816, 23, doi: [10.3847/0004-637X/816/1/23](https://doi.org/10.3847/0004-637X/816/1/23)
- Simionescu, A., Werner, N., Böhringer, H., et al. 2009, *A&A*, 493, 409, doi: [10.1051/0004-6361:200810225](https://doi.org/10.1051/0004-6361:200810225)
- Springob, C. M., Haynes, M. P., Giovanelli, R., & Kent, B. R. 2005, *ApJS*, 160, 149, doi: [10.1086/431550](https://doi.org/10.1086/431550)
- Stasińska, G., Vale Asari, N., Cid Fernandes, R., et al. 2008, *MNRAS*, 391, L29, doi: [10.1111/j.1745-3933.2008.00550.x](https://doi.org/10.1111/j.1745-3933.2008.00550.x)
- Storchi-Bergmann, T., Schmitt, H. R., Calzetti, D., & Kinney, A. L. 1998, *AJ*, 115, 909, doi: [10.1086/300242](https://doi.org/10.1086/300242)
- Sutherland, R., Dopita, M., Binette, L., & Groves, B. 2018, *MAPPINGS V: Astrophysical plasma modeling code*, Astrophysics Source Code Library, record ascl:1807.005 <http://ascl.net/1807.005>
- Thomas, A. D., Groves, B. A., Sutherland, R. S., et al. 2016, *ApJ*, 833, 266, doi: [10.3847/1538-4357/833/2/266](https://doi.org/10.3847/1538-4357/833/2/266)
- Thomas, A. D., Kewley, L. J., Dopita, M. A., et al. 2019, *ApJ*, 874, 100, doi: [10.3847/1538-4357/ab08a1](https://doi.org/10.3847/1538-4357/ab08a1)
- Tremonti, C. A., Heckman, T. M., Kauffmann, G., et al. 2004, *ApJ*, 613, 898, doi: [10.1086/423264](https://doi.org/10.1086/423264)
- Trindade Falcão, A., Fabbiano, G., Elvis, M., et al. 2025, *ApJ*, 986, 175, doi: [10.3847/1538-4357/addc64](https://doi.org/10.3847/1538-4357/addc64)
- Ulvestad, J. S., & Wilson, A. S. 1984, *ApJ*, 285, 439, doi: [10.1086/162520](https://doi.org/10.1086/162520)
- Vayner, A., Díaz-Santos, T., Ferkinhoff, C. D., et al. 2025, arXiv e-prints, arXiv:2510.09870, doi: [10.48550/arXiv.2510.09870](https://doi.org/10.48550/arXiv.2510.09870)
- Veilleux, S., & Osterbrock, D. E. 1987, *ApJS*, 63, 295, doi: [10.1086/191166](https://doi.org/10.1086/191166)
- Villar Martín, M., López Cobá, C., Cazzoli, S., Pérez Montero, E., & Cabrera Lavers, A. 2024, *A&A*, 690, A397, doi: [10.1051/0004-6361/202449621](https://doi.org/10.1051/0004-6361/202449621)
- Zhu, P., Kewley, L. J., & Sutherland, R. S. 2023, *ApJ*, 954, 175, doi: [10.3847/1538-4357/acd757](https://doi.org/10.3847/1538-4357/acd757)
- Zhu, P., Kewley, L. J., & Sutherland, R. S. 2024, *ApJ*, 977, 187, doi: [10.3847/1538-4357/ad8f37](https://doi.org/10.3847/1538-4357/ad8f37)
- Zhu, P., Kewley, L. J., Sutherland, R. S., & Grasha, K. 2025, *ApJ*, 988, 261, doi: [10.3847/1538-4357/ade78f](https://doi.org/10.3847/1538-4357/ade78f)